Andreev spectroscopy and surface density of states for a three-dimensional time-reversal invariant topological superconductor

Andreas P. Schnyder, 1, * P. M. R. Brydon, 2, † Dirk Manske, 1 and Carsten Timm²

¹Max-Planck-Institut für Festkörperforschung, Heisenbergstrasse 1, D-70569 Stuttgart, Germany ²Institut für Theoretische Physik, Technische Universität Dresden, 01062 Dresden, Germany (Dated: June 8, 2018)

A topological superconductor is a fully gapped superconductor that exhibits exotic zero-energy Andreev surface states at interfaces with a normal metal. In this paper we investigate the properties of a three-dimensional time reversal invariant topological superconductor by means of a two-band model with unconventional pairing in both the inter- and intraband channels. Due to the bulk-boundary correspondence the presence of Andreev surface states in this system is directly related to the topological structure of the bulk wavefunctions, which is characterized by a winding number. Using quasiclassical scattering theory we construct the spectrum of the Andreev bound states that appear near the surface and compute the surface density of states for various surface orientations. Furthermore, we consider the effects of band splitting, i.e., the breaking of an inversion-type symmetry, and demonstrate that in the absence of band splitting there is a direct transition between the fully gapped topologically trivial phase and the nontrivial phase, whereas in the presence of band splitting there exists a finite region of a gapless nodal superconducting phase between the fully gapped topologically trivial and nontrivial phases.

PACS numbers: 73.43.-f, 73.20.At, 73.20.Fz, 74.25.Fy

I. INTRODUCTION

Due to the recent experimental discovery of the quantum spin Hall effect¹⁻⁴ and the three-dimensional, spin-orbit induced \mathbb{Z}_2 topological insulator,^{5–9} there has been a surge of interest in the study of topological insulating electronic phases. Parallel to these developments, many workers have examined topological superconductors, 10-22 which are fully gapped unconventional superconductors that exhibit exotic gapless Andreev surface states. Both topological insulators and topological superconductors can be described within a unified mathematical framework, 11,15,16,22 which provides a complete and exhaustive classification of topological phases of gapped free fermion systems in terms of discrete symmetries and spatial dimension. A distinctive property of these states is the bulkboundary correspondence, which connects the presence of delocalized boundary modes to the topological structure of the bulk wavefunctions.

Notable examples of topological superconductors include the spinless chiral (p_x+ip_y) -wave superconductor²³ and the B phase of superfluid ${}^3\mathrm{He.}{}^{11,12,17}$ Here we focus on another type of topological superconductor, which has been largely overlooked so far, namely the three-dimensional superconductor in symmetry class CI in the terminology adopted by Ref. 11 (following the Altland-Zirnbauer classification^{24,25}). The distinguishing characteristic of the CI topological superconductor is that, unlike any of the other three-dimensional topological states, it possesses a form of SU(2) spin- or pseudospin-rotation symmetry. In Ref. 14 a tight-binding model on the diamond lattice was proposed that realizes this nontrivial topological phase.

In this paper we recast the model of Ref. 14 into a form in which the topology of the Bogoliubov-de Gennes Hamiltonian is completely determined by the phase structure of the superconducting gaps near the normal state Fermi surfaces. That is, we consider a two-band superconductor with exotic inter- and intraband gap functions, whose topological characteristics do not depend on the full Brillouin zone, but are controlled entirely by the properties of both the inter- and intraband gaps in the neighborhood of the Fermi surfaces. The reason for considering this case is two-fold: (i) It provides a clear interpretation of the topological properties in terms of the phase winding of the superconducting gap functions and (ii) it allows for the straightforward application of the tools of quasiclassical scattering theory, a technique which has proven to be extremely useful for the study of the pairing symmetry in unconventional superconductors. 26-31 Within this formalism, both the surface density of states and the spectrum of the Andreev bound states can be readily computed. It is known that in some unconventional superconductors the presence of sub-gap surface bound states leads to zero-energy anomalies in the surface density of states.^{28–31} We will see that this rule also applies to the CI topological superconductor.

The remainder of the paper is organized as follows. Section II describes the model Hamiltonian and its symmetries. In Section III we introduce a bulk topological invariant and compute the phase diagram as a function of band width and chemical potential. Section IV is concerned with the Andreev bound state spectrum and the surface density of states for various surface orientations. We conclude with a summary and discussion in Section V.

II. MODEL HAMILTONIAN AND SYMMETRIES

Our starting point is a time-reversal invariant two-band superconductor on a simple cubic lattice with inter- and intraband pairing, which has the form of a 4×4 Bogoliubov-de Gennes Hamiltonian. The mean-field Hamiltonian $\mathcal{H}=$

 $\sum_{k} \Psi_{k} H(k) \Psi_{k}^{\dagger}$ is diagonal in momentum space with

$$H(\mathbf{k}) = \begin{pmatrix} h(\mathbf{k}) & \delta(\mathbf{k}) \\ \delta^{\dagger}(\mathbf{k}) & -h^{T}(-\mathbf{k}) \end{pmatrix}$$
(1a)

and $\Psi_{\boldsymbol{k}}=(a_{\boldsymbol{k}\uparrow},b_{\boldsymbol{k}\uparrow},a_{-\boldsymbol{k}\downarrow}^{\dagger},b_{-\boldsymbol{k}\downarrow}^{\dagger})^{T}$, where $a_{\boldsymbol{k}\sigma}$ and $b_{\boldsymbol{k}\sigma}$ denote electron annihilation operators with spin σ and momentum \boldsymbol{k} for band one and two, respectively. The normal state Hamiltonian $h(\boldsymbol{k})$ and the gap matrix $\delta(\boldsymbol{k})$ are given by

$$h(\mathbf{k}) = \begin{pmatrix} \Theta_{1\mathbf{k}} & 0 \\ 0 & \Theta_{2\mathbf{k}} \end{pmatrix}$$
 and $\delta(\mathbf{k}) = \begin{pmatrix} \Delta_{\mathbf{k}} & \Phi_{\mathbf{k}} \\ \Phi_{\mathbf{k}}^* & -\Delta_{\mathbf{k}} \end{pmatrix}$, (1b)

respectively. Here, the band dispersions are

$$\Theta_{jk} = t_j \left(\cos k_x + \cos k_y + \cos k_z\right) - \mu_j, \quad (1c)$$

with j = 1, 2, the intraband pairing potential is

$$\Delta_{\mathbf{k}} = \Delta_d \left(\cos k_x - \cos k_y\right) + \Delta_s,\tag{1d}$$

and the interband pairing potential takes the form³²

$$\Phi_{\mathbf{k}} = \Phi_0 \left(\sin k_x \sin k_y + i \sin k_z \right). \tag{1e}$$

We observe that Hamiltonian (1) is closely related to the model of Ref. 14. Specifically, by performing a particle-hole transformation the tight-binding Hamiltonian analyzed in Ref. 14 can be brought into a form in which the momentum dependence of the gap functions along the Fermi surface have the same topology as the pairing potentials in Eq. (1a). We note, however, that the present model is defined on a simple cubic lattice, whereas in Ref. 14 a diamond lattice was considered. The energy spectrum of H(k) is composed of four bands with energies $E(k) \in \{-\Lambda_{1k}, -\Lambda_{2k}, +\Lambda_{1k}, +\Lambda_{2k}\}$ and

$$\Lambda_{1k} = \sqrt{\Delta_k^2 + \frac{1}{4} \left[\Theta_{1k} - \Theta_{2k} + B_k\right]^2},$$

$$\Lambda_{2k} = \sqrt{\Delta_k^2 + \frac{1}{4} \left[\Theta_{1k} - \Theta_{2k} - B_k\right]^2},$$
(2)

where
$$B_{\mathbf{k}} = \sqrt{4 \left| \Phi_{\mathbf{k}} \right|^2 + (\Theta_{1\mathbf{k}} + \Theta_{2\mathbf{k}})^2}$$
.

A topological superconductor belonging to the symmetry class CI satisfies two independent *antiunitary* symmetries: time-reversal symmetry $\mathcal{T}=KU_T$, with $\mathcal{T}^2=+1$, and particle-hole symmetry $\mathcal{C}=KU_C$, with $\mathcal{C}^2=-1$. Here, K denotes the complex conjugation operator. For the above example, time-reversal symmetry is expressed as

$$U_T H^*(-\mathbf{k}) U_T^{\dagger} = +H(\mathbf{k}), \tag{3a}$$

where $U_T=\mathbb{1}$ is the 4×4 identity matrix. The particle-hole symmetry can be expressed as 33

$$U_C H^*(-\mathbf{k}) U_C^{\dagger} = -H(\mathbf{k}), \tag{3b}$$

with $U_C = i\sigma_2 \otimes \sigma_0$. Here, and in the following, $\sigma_{1,2,3}$ denote the three Pauli matrices and σ_0 is the 2×2 unit matrix. By combining Eq. (3a) with Eq. (3b) we find that the

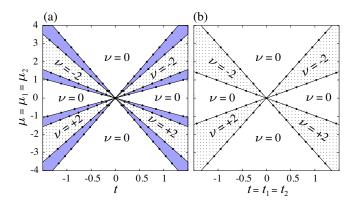


FIG. 1: (color online). Phase diagram for the CI topological superconductor, Eq. (1), as a function of bandwidth and chemical potential with $\Phi_0=0.4,\,\Delta_d=0.4,$ and $\Delta_s=0.$ The gapped phases are characterized by the even-numbered winding number $\nu,$ Eq. (10). Blue areas are bulk gapless phases. (a) Inversion asymmetric case with split bands, $t_1=t,\,t_2=0.9t$ and $\mu_1=\mu_2.$ (b) Inversion symmetric case with degenerate bands, $t_1=t_2$ and $\mu_1=\mu_2.$

gap matrix $\delta(\mathbf{k})$ is required to be Hermitian, $\delta^{\dagger}(\mathbf{k}) = \delta(\mathbf{k})$. Besides particle-hole and time-reversal symmetry, Hamiltonian (1) satisfies another symmetry which is given by

$$S^{\dagger}H(\mathbf{k})S = -H(\mathbf{k}),\tag{3c}$$

with $S=iU_TU_C=-\sigma_2\otimes\sigma_0$. That is, H(k) anti-commutes with the "chiral" symmetry operator S. The significance of symmetry (3c) is that it allows us to bring the Hamiltonian into block off-diagonal form. Namely, we find that in the basis in which S is diagonal, $\tilde{S}=WSW^{\dagger}=\mathrm{diag}\left(-\sigma_0,+\sigma_0\right)$, the Hamiltonian H(k) takes the form

$$\tilde{H}(\mathbf{k}) = WH(\mathbf{k})W^{\dagger} = \begin{pmatrix} 0 & D(\mathbf{k}) \\ D^{\dagger}(\mathbf{k}) & 0 \end{pmatrix},$$
 (4)

with the off-diagonal component

$$D(\mathbf{k}) = h(\mathbf{k}) - i\delta(\mathbf{k}),\tag{5}$$

and the unitary transformation

$$W = \frac{1}{\sqrt{2}} \begin{pmatrix} \sigma_0 & -i\sigma_0 \\ \sigma_0 & +i\sigma_0 \end{pmatrix}. \tag{6}$$

The block off-diagonal form (4) is particularly useful to uncover the topological properties of the ground state wavefunctions, as we will explain below.

We end this Section by discussing the case of degenerate bands in Eq. (1), i.e., $\Theta(\mathbf{k}) \equiv \Theta_1(\mathbf{k}) = \Theta_2(\mathbf{k})$. This condition leads to an additional symmetry of $H(\mathbf{k})$,

$$U_p H(-\mathbf{k}) U_p^{\dagger} = H(\mathbf{k}), \tag{7}$$

with the unitary matrix $U_p = \sigma_3 \otimes \sigma_2$. Eq. (7) represents a type of inversion symmetry, as it is a *unitary* symmetry that relates Bogoliubov-de Gennes Hamiltonians at +k and

-k via a transformation that interchanges the two bands. With symmetry (7) the energy spectrum becomes degenerate and takes the simple form $E(k) \in \{-\Lambda_k, +\Lambda_k\}$ with $\Lambda_k = \sqrt{\Theta_k^2 + \Delta_k^2 + |\Phi_k|^2}$.

III. WINDING NUMBER AND PHASE DIAGRAM

To determine the topological properties of the model under consideration we first introduce an integer topological invariant, the winding number ν . 11,15 In order to do so it is convenient to adiabatically deform H(k) into a flat-band Hamiltonian. This can be achieved by means of a singular value decomposition. First of all we note that for the off-diagonal block D(k), Eq. (5), which is in general non-Hermitian, there exists a factorization of the form $D(\mathbf{k}) = U^{\dagger}(\mathbf{k})\Sigma(\mathbf{k})V(\mathbf{k})$, where $\Sigma(k)$ is a diagonal matrix with positive real numbers on the diagonal and U(k) and V(k) are unitary matrices. Direct calculation shows that the eigenvalues of $\Sigma(k)$ are identical to the positive eigenvalues of the Bogoliubov-de Gennes Hamiltonian H(k). For a fully gapped superconductor, it is possible to adiabatically deform the spectrum into flat bands with eigenvalues +1 and -1. This procedure amounts to replacing $\Sigma(k)$ by the unit matrix. Hence, the flat-band Hamiltonian $Q(\mathbf{k})$ in the off-diagonal basis reads

$$Q(\mathbf{k}) = \begin{pmatrix} 0 & q(\mathbf{k}) \\ q^{\dagger}(\mathbf{k}) & 0 \end{pmatrix}, \tag{8}$$

with the unitary matrix $q(\mathbf{k}) = U^{\dagger}(\mathbf{k})V(\mathbf{k})$. In terms of the gap functions and band dispersions of model (1), the off-diagonal block of the flat-band Hamiltonian is given by

$$q(\mathbf{k}) = \begin{pmatrix} \Lambda_{+}B_{\mathbf{k}} - \Lambda_{-}\Theta_{+} & -2i\Lambda_{-}\Phi_{\mathbf{k}} \\ +2i\Lambda_{-}\Phi_{\mathbf{k}}^{*} & \Lambda_{+}B_{\mathbf{k}} + \Lambda_{-}\Theta_{+} \end{pmatrix} \frac{D(\mathbf{k})/2}{\Lambda_{1\mathbf{k}}\Lambda_{2\mathbf{k}}B_{\mathbf{k}}},$$
(9)

where $\Lambda_{\pm} = \Lambda_{1k} \pm \Lambda_{2k}$ and $\Theta_{+} = \Theta_{1k} + \Theta_{2k}$. As a consequence of time-reversal invariance $q(\mathbf{k})$ satisfies $q^{T}(-\mathbf{k}) = q(\mathbf{k})$. The topological invariant characterizing CI topological superconductors is defined as the winding number of the off-diagonal block $q(\mathbf{k})$, $q(\mathbf{k})$,

$$\nu = \frac{1}{24\pi^2} \int d^3k \, \varepsilon^{\mu\nu\rho} \, \text{Tr} \left[\left(q^{-1} \partial_{\mu} q \right) \left(q^{-1} \partial_{\nu} q \right) \left(q^{-1} \partial_{\rho} q \right) \right], \tag{10}$$

where the integral is over the first Brillouin zone. From the constraint $q^T(-{\bm k})=q({\bm k})$ it follows that ν is even.

Next we use the topological invariant (10) to analyze the phase diagram of $H(\boldsymbol{k})$, Eq. (1), as a function of chemical potential and band width. Fully gapped phases with different topological properties are separated by regions (or lines) of nodal superconducting phases (see Fig. 1). The condition for the existence of a gapless phase can be expressed in terms of a vanishing determinant, i.e., $\det H(\boldsymbol{k}) = -|\det D(\boldsymbol{k})|^2 = 0$. By use of Eq. (1b) and Eq. (5) we obtain

$$\Delta_{\mathbf{k}}^{2} + |\Phi_{\mathbf{k}}|^{2} + \Theta_{1\mathbf{k}}\Theta_{2\mathbf{k}} = 0, \quad \Delta_{\mathbf{k}} (\Theta_{1\mathbf{k}} - \Theta_{2\mathbf{k}}) = 0.$$
 (11)

Let us first focus on the inversion asymmetric case with split bands, $\Theta_{1k} \neq \Theta_{2k}$. The above two conditions then reduce to

$$\Delta_{\mathbf{k}} = 0, \quad |\Phi_{\mathbf{k}}|^2 = -\Theta_{1\mathbf{k}}\Theta_{2\mathbf{k}}.\tag{12}$$

Provided $\operatorname{sgn} \Theta_{1k} = -\operatorname{sgn} \Theta_{2k}$, Eqs. (12) have solutions describing nodal rings that appear in the gapless phase of Fig. 1(a) (blue shaded area). These gap-closing lines in momentum space are topologically stable and are characterized by an integer topological charge, ³⁴ akin to the band touching points in graphene. That is, the appearance of these nodal lines is generic and stable against (small) perturbations of the Hamiltonian, such as, e.g., the inclusion of higher d-wave gap harmonics in the intraband pairing potential.

In the presence of inversion symmetry (7), with $\Theta_{k} \equiv$ $\Theta_{1k} = \Theta_{2k}$, the gap closing condition (11) becomes Δ_k^2 + $|\Phi_{\mathbf{k}}|^2 + \Theta_{\mathbf{k}}^2 = 0$. Hence, there are in general four conditions that need to be satisfied for the gap to be zero, which exceeds the number of free parameters (k_x, k_y, k_z) . In other words, if we consider tuning a single parameter, e.g., the band width t, to drive a transition from a topologically nontrivial phase to a topologically trivial phase, a gap closing can only occur at isolated points in the (k, t) parameter space [see Fig. 1(b)]. Thus, the presence of inversion symmetry (7) leads to a direct quantum phase transition between two distinct gapped phases (i.e, there is no intervening gapless phase). The phase boundaries in the (t, μ) -plane are given by $\mu = \pm t$ and $\mu = \pm 3t$, as shown in Fig. 1(b). The fact that direct transitions from one gapped phase to another are only possible in the presence of inversion symmetry is a feature which is common to threedimensional topological phases.³⁴ In particular, it also occurs in \mathbb{Z}_2 topological insulators.³⁵

To determine the topological nature of the eight gapped phases in Fig. 1 (white and dotted areas), we computed the winding number ν numerically, by discretizing the integral (10) over the Brillouin zone. It turns out that four phases are topologically nontrivial with winding number $\nu=\pm 2$. In these nontrivial phases, there appear linearly dispersing, midgap surface states when the system is placed next to a normal metal or insulating state. These exotic Andreev bound states are robust against localization from random impurities. We will study these surface states in more detail in Section IV. In passing, we note that for the inversion symmetric case of model (1), there exists an intimate connection between the topological properties of the Bogoliubov-de Gennes wavefunctions, as characterized by the winding number ν , and the Fermi surface topology in the normal state. In particular, the transition from a topologically trivial to a nontrivial phase in Fig. 1(b) coincides with a change in Fermi surface topology. A similar relationship has been previously reported for fully gapped time-reversal invariant spin-triplet superconductors. 18

A. Fermi surface topological invariant

An important property of Hamiltonian (1) is that in the presence of inversion symmetry its topological characteristics are completely determined by the momentum dependence of the superconducting gap functions along the normal-state Fermi

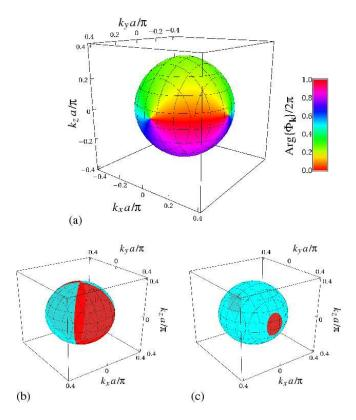


FIG. 2: (color online). Panel (a): Variation of $\arg(\Phi_k)$ over the Fermi surface. The argument of Φ_k shows four distinct singularities on the Fermi surface. The locations of these singularities are related by a four-fold rotational symmetry about the z axis. Panel (b) and (c): Variation of $\mathrm{sign}(\Delta_k)$ over the Fermi surface. Red indicates $\mathrm{sign}(\Delta_k)=+1$, while blue is $\mathrm{sign}(\Delta_k)=-1$. The ratio between s- and d- wave components is $\Delta_s/\Delta_d=0$ and $\Delta_s/\Delta_d=3/7$ in panel (b) and (c), respectively. The normal state band structure parameters are $t_1=t_2=1$ and $\mu_1=\mu_2=1.75$.

surface. To demonstrate this, we give an illustration of the topological properties of $H(\boldsymbol{k})$ in terms of the phase structure of the gap functions on the Fermi surface.

For definitiveness we consider a Fermi surface of spherical topology which is centered around the Γ point, k = 0, i.e. we focus on the region $t < \mu < 3t$ in the (t, μ) -plane of Fig. 1(b). In the following we will hold the band structure parameters tand μ fixed and use the ratio between s- and d-wave components in the intraband pairing (1d) to tune the system form a topologically trivial to a nontrivial phase. Projected onto the Fermi surface, we find that $\Phi(k)$ has four first-order zeroes at momenta $k_{1\pm} = (\pm k_F, 0, 0)$ and $k_{2\pm} = (0, \pm k_F, 0)$, with associated singularities in $arg(\Phi_k)$ [see Fig. 2(a)]. In other words, the real vector field Φ_k over the Fermi surface exhibits vortices at ${m k}_{1\pm}$ and anti-vortices at ${m k}_{2\pm}$ with winding number +1 and -1, respectively. The appearance of vortices in $\Phi(k)$ is a necessary but not sufficient condition for the nontriviality of the model. What is required in addition is that $\Delta(\mathbf{k})$ reverses sign between vortices of $\Phi(\mathbf{k})$ with opposite winding number. Figs. 2(b) and 2(c) display the variation of the sign of $\Delta(k)$ over the Fermi surface for two different parameter choices, which both lead to a nontrivial state. For $\Delta_d\cos(k_F)>\Delta_s$ the sign of $\Delta_{\pmb k}$ reverses between $\pmb k_{1\pm}$ and $\pmb k_{2\pm}$, and the system is in the topologically nontrivial phase. If $\Delta_d\cos(k_F)<\Delta_s$, on the other hand, the sign of $\Delta_{\pmb k}$ is the same across the Fermi surface, and so we have a topologically trivial state.

IV. ANDREEV BOUND STATES AND SURFACE DENSITY OF STATES

A physical consequence of the nonzero winding number ν is the appearance of gapless Andreev bound states at the surface of a CI topological superconductor or at an interface between a normal metal and a CI topological superconductor. The bulk-boundary correspondence relates the number of Andreev bound states to the topological number ν . In this Section we derive the energy spectrum of the bound states and the surface density of states using quasiclassical scattering theory. For simplicity, we focus on the inversion symmetric case of model (1) and assume a spherically symmetric Fermi surface. But the results we obtain are expected to remain qualitatively unchanged upon inclusion of anisotropic Fermi velocities or inversion asymmetric perturbations.

As we have seen in Section III the topological characteristics of the inversion symmetric model (1) are fully determined by the phase structure of the pairing functions on the Fermi surface. This implies that we can capture the key topological structure of the superconducting state by adopting an effective low-energy quasiclassical description as long as the gap functions $\Delta(r)$ and $\Phi(r)$ are slowly varying over length scales of the order of the inverse Fermi momentum k_F^{-1} . Hence, we proceed by approximating the momentum dependence of the gap functions in the vicinity of the Fermi surface by

$$\Delta_{\mathbf{k}} = \Delta[\lambda(k_x^2 - k_y^2)/k_F^2 + (1 - \lambda)],$$
 (13)

$$\Phi_{\mathbf{k}} = \Phi(k_x k_y / k_F^2 + i k_z / k_F) = |\Phi_{\mathbf{k}}| e^{i \varphi_{\mathbf{k}}}. \tag{14}$$

Here we have introduced the parameter λ to tune $\Delta_{\boldsymbol{k}}$ from $d_{x^2-y^2}$ -wave symmetry ($\lambda=1$, topologically nontrivial) to s-wave symmetry ($\lambda=0$, topologically trivial).

We can now apply standard methods to obtain the surface bound states. 27 We describe the system in terms of coordinates parallel (r_{\parallel}) and normal (x_{\perp}) to the interface. We assume that the superconductor occupies the region defined by $x_{\perp}>0$. We solve the Andreev equations using the ansatz

$$\Psi(\mathbf{k}_{\parallel}, \mathbf{r}) = \sum_{j=1}^{4} \alpha_{j} \Psi_{j}(\mathbf{k}_{\parallel}, \mathbf{r})$$
 (15)

for the wavefunctions of a bound state of energy E, where the spinors are written

$$\Psi_1(\boldsymbol{k}_{\parallel}, \boldsymbol{r}) = \begin{pmatrix} 1, 0, u_{\boldsymbol{k}}, v_{\boldsymbol{k}} \end{pmatrix}^T e^{i\boldsymbol{k}\cdot\boldsymbol{r}} e^{-\kappa_{\boldsymbol{k}}x_{\perp}}$$
 (16a)

$$\Psi_2(\boldsymbol{k}_{\parallel}, \boldsymbol{r}) = \begin{pmatrix} 1, & 0, & u_{\tilde{\boldsymbol{k}}}, & v_{\tilde{\boldsymbol{k}}} \end{pmatrix}^T e^{i\tilde{\boldsymbol{k}}\cdot\boldsymbol{r}} e^{-\kappa_{\tilde{\boldsymbol{k}}}x_{\perp}}$$
 (16b)

$$\Psi_3(\boldsymbol{k}_{\parallel}, \boldsymbol{r}) = \begin{pmatrix} 0, 1, v_{\boldsymbol{k}}, -u_{\boldsymbol{k}} \end{pmatrix}^T e^{i\boldsymbol{k}\cdot\boldsymbol{r}} e^{-\kappa_{\boldsymbol{k}}x_{\perp}}$$
 (16c)

$$\Psi_4(\boldsymbol{k}_{\parallel},\boldsymbol{r}) \ = \ \left(\ 0, \ 1, \ v_{\tilde{\boldsymbol{k}}}, \ -u_{\tilde{\boldsymbol{k}}} \ \right)^T e^{i\tilde{\boldsymbol{k}}\cdot\boldsymbol{r}} e^{-\kappa_{\tilde{\boldsymbol{k}}}x_{\perp}} (16\mathrm{d})$$

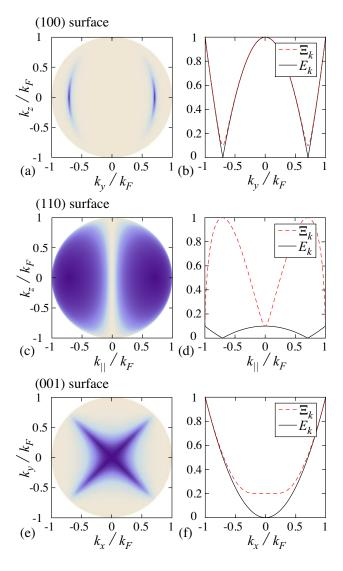


FIG. 3: (color online). Panels (a), (c), and (e): Energy of the upper branch of the interface states E_k [see Eq. (18)] as a fraction of the gap amplitude Ξ_k for (a) the (100) interface perpendicular to \hat{e}_x , (c) the (110) interface perpendicular to $\frac{1}{\sqrt{2}}(\hat{e}_x + \hat{e}_y)$, and (e) the (001) interface perpendicular to \hat{e}_z . The color scale is such that blue corresponds to $E_{\mathbf{k}}/\Xi_{\mathbf{k}}=0$, while grey is $E_{\mathbf{k}}/\Xi_{\mathbf{k}}=1$. Panels (b), (d), and (f): Comparison of the Andreev state dispersion E_k and the bulk gap Ξ_k for the same interface configurations as in panels (a), (c), and (e), respectively. In all panels we take $\Delta_d = 1$, $\Delta_s = 0$ and $\Phi_0 = 0.2.$

with

$$u_{\boldsymbol{p}} = \frac{\Delta_{\boldsymbol{p}}}{\Xi_{\boldsymbol{p}}^2} \left[E - i \frac{p_{\perp}}{|p_{\perp}|} \sqrt{\Xi_{\boldsymbol{p}}^2 - E^2} \right] , \qquad (17a)$$

$$v_{p} = \frac{\Phi_{p}}{\Xi_{p}^{2}} \left[E + i \frac{p_{\perp}}{|p_{\perp}|} \sqrt{\Xi_{p}^{2} - E^{2}} \right],$$
 (17b)

$$\kappa_{\boldsymbol{p}} = \frac{1}{|v_F^{x_\perp}|} \sqrt{\Xi_{\boldsymbol{p}}^2 - E^2}, \qquad (17c)$$

and $v_F = \partial \Theta_p / \partial p$ denotes the Fermi velocity. We define

the wavevectors ${m k}=({m k}_\parallel,k_\perp)$ and ${m k}=({m k}_\parallel,-k_\perp)$ with the requirement that $|\mathbf{k}| = |\tilde{\mathbf{k}}| = k_F$.

The energy of the bound states is obtained by the condition that the equation $\Psi(\mathbf{k}_{\parallel}, \mathbf{r})|_{x_{\perp}=0} = 0$ has a nontrivial solution for the coefficients α_i . Although in general this yields a rather complicated expression for the bound state energies, we can simplify matters considerably if we assume that $|\Delta_{k}| = |\Delta_{\tilde{k}}|$ and $|\Phi_{\boldsymbol{k}}| = |\Phi_{\tilde{\boldsymbol{k}}}|$, which holds for certain high-symmetry reflection planes. We hence find the bound state energies

$$E_{\boldsymbol{k}_{\parallel}}^{2} = \frac{1}{2} \left[\Xi_{\boldsymbol{k}}^{2} + \Delta_{\boldsymbol{k}} \Delta_{\tilde{\boldsymbol{k}}} + |\Phi_{\boldsymbol{k}}|^{2} \cos(\varphi_{\boldsymbol{k}} - \varphi_{\tilde{\boldsymbol{k}}}) \right]. (18)$$

This expression is valid in both the topologically trivial and nontrivial cases. A zero-energy state is possible whenever the following two conditions are both satisfied

$$\begin{split} \text{(i)} & |\Phi_{\pmb{k}}| = 0 \quad \text{or} \quad \cos(\varphi_{\pmb{k}} - \varphi_{\tilde{\pmb{k}}}) = -1, \\ \text{(ii)} & |\Delta_{\pmb{k}}| = 0 \quad \text{or} \quad \operatorname{sgn} \Delta_{\pmb{k}} \operatorname{sgn} \Delta_{\tilde{\pmb{k}}} = -1. \quad \text{(} \end{split}$$

(ii)
$$|\Delta_{\mathbf{k}}| = 0$$
 or $\operatorname{sgn} \Delta_{\mathbf{k}} \operatorname{sgn} \Delta_{\tilde{\mathbf{k}}} = -1$. (19)

We shall illustrate different possible combinations of these conditions for the appearance of the zero-energy states by examining three distinct cases: the (100) surface, the (110) surface, and the (001) surface.

The surface bound states in unconventional superconductors can be observed by scanning tunneling spectroscopy of the surface density of states (SDOS). It is therefore interesting to consider the SDOS for our three surfaces, in order to determine the experimentally relevant signatures of the topologically nontrivial phase. To obtain the SDOS we must first calculate the quasiclassical retarded Green's function $\mathcal{G}_{\mathbf{k}_{\parallel}}^{r}(\mathbf{r},\mathbf{r}';E)$. This will not be explicitly constructed here as it is rather laborious; for a detailed discussion see Ref. 30 and references therein. Because we are dealing with a twoband system, the quasiclassical Green's function \mathcal{G} will be a 4×4 matrix in the Nambu-band space. The SDOS is simply the local density of states (DOS) at the surface of the superconductor, where the local DOS at the point r is defined as

$$\rho(E, \boldsymbol{r}) = -\frac{1}{\pi} \sum_{\boldsymbol{k}_{\parallel}} \operatorname{Im} \left\{ \mathcal{G}_{\boldsymbol{k}_{\parallel}}^{r,11}(\boldsymbol{r}, \boldsymbol{r}; \widetilde{E}) + \mathcal{G}_{\boldsymbol{k}_{\parallel}}^{r,22}(\boldsymbol{r}, \boldsymbol{r}; \widetilde{E}) \right\}. \tag{20}$$

Here $\mathcal{G}^{r,11}$ and $\mathcal{G}^{r,22}$ are the electron-like Green's functions for bands one and two, respectively, and $E = E + i\Gamma$ contains the phenomenological broadening parameter Γ . In all our calculations we set $\Gamma = 0.01\Delta$.

(100) surface

We consider first the appearance of zero-energy states at the (100) surface for $\lambda = 1$. From the conditions Eq. (19) on the intraband pairing we have $\mathrm{sgn}\Delta_{m{k}}\mathrm{sgn}\Delta_{\widetilde{m{k}}}=1$ for all k, but $\Delta_k = 0$ along the lines defined by $k = (k_x, \pm k_x, k_z)$. The interband potential is always non-zero for these momenta, but we do have $\cos(\varphi_{\pmb{k}}-\varphi_{\widetilde{\pmb{k}}})=-1$ (i.e. a sign reversal of $\Phi_{\bf k}$ upon reflection) whenever $k_z=0$. We hence obtain two zero-energy states at ${\bf k}_1=(k_F/\sqrt{2},k_F/\sqrt{2},0)$ and $\mathbf{k}_2 = (k_F/\sqrt{2}, -k_F/\sqrt{2}, 0)$. These arguments still hold if we decrease λ towards 0.5, but the momenta \mathbf{k}_1 and \mathbf{k}_2 will move towards one another, eventually merging at $\lambda = 0.5$ where we have a gapless state.

In Fig. 3(a) we plot the $\lambda=1$ surface states in units of Ξ_k . The energy of the surface states only deviates significantly from the bulk gap close to the nodal lines of Δ_k ; this is clearly visible in the $k_z=0$ cut through the surface states shown in Fig. 3(b).

The SDOS is shown in Fig. 4(a) for fixed $\lambda=1$ and various values of Φ . At $\Phi=0$ we recover the SDOS for a 3D $d_{x^2-y^2}$ superconductor. For non-zero Φ we observe that at low energies the SDOS is linear with a slope that is controlled by the velocity of the 2D linearly-dispersing surface states. The minimum energy of the bulk gap is located at $E=0.5\Phi$, which is visible in the SDOS as the point where the energy dependence becomes superlinear. The linear slope of the low-energy SDOS does not change with increasing Φ , indicating that the velocity of the linear-dispersing surface states is mainly determined by Δ . We note that the finite SDOS at E=0 is an artifact of the broadening parameter.

As shown in Fig. 4(b), the SDOS is qualitatively different in the topologically trivial ($\lambda < 0.5$) and the nontrivial ($\lambda > 0.5$) regimes. In the former the low-energy SDOS is vanishing within the gap, while in the latter there is the characteristic linear energy dependence. Note that the sharp spike at $E = \Delta$ in the $\lambda = 0$ curve is the DOS peak associated with the purely s-wave intraband gap.

B. (110) surface

We now examine the bound states at the (110) surface. Again setting $\lambda=1$, we see that the condition $\operatorname{sgn}(\Delta_{\pmb{k}})\operatorname{sgn}(\Delta_{\widehat{\pmb{k}}})=-1$ on the intraband potential is satisfied for all \pmb{k} . A zero-energy state thus only requires that $\Phi_{\pmb{k}}$ vanishes for some \pmb{k} or that $\cos(\varphi_{\pmb{k}}-\varphi_{\widehat{\pmb{k}}})=-1$. The former holds for $\pmb{k}_1=(k_F,0,0)$ and $\pmb{k}_2=(0,k_F,0)$, while the latter is never realized. Compared to the (100) surface the roles of $\Delta_{\pmb{k}}$ and $\Phi_{\pmb{k}}$ are reversed: the zero-energy states are realized because $\Phi_{\pmb{k}}$ vanishes at momenta where $\Delta_{\pmb{k}}$ has a sign change upon reflection. Furthermore, the position of the zero-energy states do not change for $1>\lambda>0.5$, as the sign change of $\Delta_{\pmb{k}}$ at \pmb{k}_1 and \pmb{k}_2 survives while the zeros of $\Phi_{\pmb{k}}$ remain the same.

The energy of the $\lambda=1$ surface states is shown in units of the bulk gap in Fig. 3(c). In contrast to the (100) surface, most of the interface states have energies differing significantly from $\Xi_{\bf k}$. This can be understood as being due to the sign reversal upon reflection of $\Delta_{\bf k}$, which for $\Phi_{\bf k}=0$ would give dispersionless zero-energy states for all ${\bf k}.^{27,30}$ In Fig. 3(d) we show a $k_z=0$ cut of the interface states and bulk gap.

In Fig. 4(c) we show the change in the SDOS upon varying Φ at fixed $\lambda=1$. Similarly to the (100) surface, at $\Phi=0$ we recover the results for a 3D d_{xy} superconductor; note that the divergence of the SDOS at E=0 is due to the zero-energy state for all \mathbf{k}_{\parallel} . As Φ is increased from zero, the SDOS becomes finite at E=0 and increases linearly with E up to a

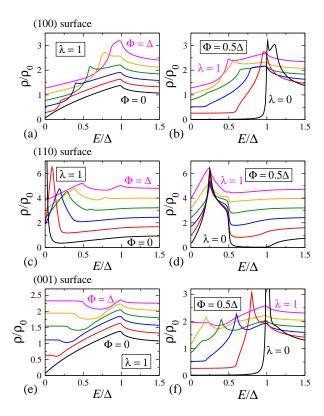


FIG. 4: (color online) SDOS at the three surfaces as a function of the energy E, normalized by the constant SDOS ρ_0 of the normal state. (100) surface: (a) fixed $\lambda=1$ and different values of $\Phi=0.2n\Delta$, and (b) fixed $\Phi=0.5\Delta$ and different $\lambda=0.2n$, offset by 0.25n, $n=0\ldots 5$. (110) surface: (c) fixed $\lambda=1$ and different values of $\Phi=0.2n\Delta$, and (d) fixed $\Phi=0.5\Delta$ and different $\lambda=0.2n$, offset by 0.75n, $n=0\ldots 5$. (001) surface: (e) fixed $\lambda=1$ and different values of $\Phi=0.2n\Delta$, and (f) fixed $\Phi=0.5\Delta$ and different $\lambda=0.2n$, offset by 0.25n, $n=0\ldots 5$.

maximum at the edge of the bulk gap. The low-energy linear slope of the SDOS decreases with increasing Φ , revealing that the velocity of the Dirac states increases with Φ . This is anticipated by the result that for this geometry the surface bound states appear about the zeroes of Φ_k .

The change in the SDOS as λ is tuned through the topological transition is more subtle than for the (100) surface. As can be seen in Fig. 4(d), there is relatively little change in the low-energy SDOS, with the main feature being that the peak at $E=0.5\Phi$ becomes sharper as λ is decreased. At $\lambda<1$ we note a drop in the SDOS at $E=0.5\Delta$; in the topologically nontrivial state, the SDOS is finite on both sides of the drop, while in the trivial state it is zero on the higher-energy side. That is, the large feature in the SDOS at $E<0.5\Delta$ in the topologically trivial state is due to surface bound states with non-zero energy.

\mathbf{C} . (001) surface

As there is no sign change of $\Delta_{\pmb{k}}$ upon reflection from the (001) surface, the zero-energy states must be located along the nodal lines of $\Delta_{\pmb{k}}$. The interband pairing potential $\Phi_{\pmb{k}}$ does not vanish for these values of \pmb{k} , but the condition $\cos(\varphi_{\pmb{k}}-\varphi_{\pmb{\tilde{k}}})=-1$ is fulfilled when the real part of $\Phi_{\pmb{k}}$ vanishes, i.e. for $\pmb{k}=(k_x,0,k_z)$ and $(0,k_y,k_z)$. For $\lambda=1$ this implies a single zero-energy bound state at $\pmb{k}=(0,0,k_F)$. As for the (100) surface, the origin of this state is due to a zero in $\Delta_{\pmb{k}}$ and the sign change of $\Phi_{\pmb{k}}$ upon reflection. Upon reducing λ , the single zero-energy state at $(0,0,k_F)$ splits into two zero-energy states at the intersection of the plane $(0,k_y,k_z)$ with the nodal lines of $\Delta_{\pmb{k}}$.

The energies of the surface state deviate most significantly from the bulk along the nodal lines of Δ_k , see Fig. 3(e). Unlike the other two surfaces, the zero-energy state has quadratic dispersion at low energy, as shown by the cut along $k_x=0$ in Fig. 3(f). For $0.5<\lambda<1$, however, the two zero-energy states have linear dispersion at low energies.

The SDOS at $\lambda=1$ is qualitatively different to the other cases because the 2D quadratic surface states contribute a constant DOS, see Fig. 4(e). The height of this constant region increases with increasing Φ , so that at $\Phi=\Delta$ the gap is completely filled. The edge of the bulk gap at $E=0.5\Phi$ is signalled by the cusp feature. The constant SDOS within the bulk gap is only found at $\lambda=1$: as shown in Fig. 4(f), for $0.5<\lambda<1$ we find the low-energy linear SDOS characteristic of linearly-dispersing zero-energy states. In the topologically trivial state the SDOS is vanishing within the gap.

V. CONCLUSIONS AND OUTLOOK

In this paper we have discussed the three-dimensional CI topological superconductor introduced in Ref. 11. We constructed a concrete realization of this topological phase in terms of a two-band Bogoliubov-de Gennes Hamiltonian with unconventional inter- and intraband pairing potentials. This lattice Hamiltonian is just one example of a wider class of models that all share the same topological properties. Quite generally, one is free to add arbitrary small deformations to the Hamiltonian without changing its topological characteristics, as long as the perturbations do not close the bulk superconducting gap. While we do not know in which specific material the considered tight-binding Hamiltonian could be realized, it is a convenient canonical model that gives valuable in-

sight into interesting properties shared by general CI topological superconductors. In the presence of inversion symmetry, the topological characteristics of this two-band superconductor are fully determined by the momentum dependence of the gap functions along the Fermi surface. That is, the topological properties are independent of the electronic band structure away from the Fermi surface. We have demonstrated that the topological invariant ν (winding number) can be related to the sign reversal of the intraband gap between vortices in the interband gap with opposite winding number. This simple criterion could be used in the search for CI topological superconductors in real materials. Our results suggest to consider time-reversal invariant systems with orbital degrees of freedom, i.e., multi-band superconductors.

The CI topological superconductor has exotic Andreev bound states at its surface or at an interface with a normal metal. These gapless modes are due to the bulk topological invariant ν , which cannot change as long as the superconductor remains fully gapped in the bulk. We have used quasiclassical scattering theory to study the energy spectrum of these Andreev bound states for various surface orientations. An important measurement technique to observe Andreev bound states in unconventional superconductors is scanning tunneling spectroscopy. We therefore computed the surface density of states and demonstrated that the presence of Andreev bound states leads to pronounced anomalies at low energies in the scanning tunneling spectra. These features provide key experimental signatures of the nontrivial topological character of the system.

Furthermore, it would be interesting to investigate the effects of the topological nontriviality of the superconductor on other experimental probes, such as tunneling conductance or Josephson current. In particular, since our model lends itself to the application of quasiclassical scattering techniques, one could examine the proximity effects in a junction involving a CI topological superconductor and a normal metal or a ferromagnet, for example, or alternatively examine vortex structures. We leave these interesting questions for future work.

Acknowledgments

The authors thank S. Ryu, B. Béri, A. Ludwig, M. Sigrist, and G. Khaliullin for discussions. A.P.S. acknowledges the hospitality of the Max-Planck-Institut PKS Dresden, where part of this paper was written.

^{*} Electronic address: a.schnyder@fkf.mpg.de

[†] Electronic address: brydon@theory.phy.tu-dresden.de

¹ C. L. Kane and E. J. Mele, Phys. Rev. Lett. **95**, 226801 (2005).

² C. L. Kane and E. J. Mele, Phys. Rev. Lett. **95**, 146802 (2005).

³ B. Bernevig, T. Hughes, and S.-C. Zhang, Science **314**, 1757 (2006).

⁴ M. König, S. Wiedmann, C. Brune, A. Roth, H. Buhmann, L. Molenkamp, X. Qi, and S. Zhang, Science 318, 766 (2007).

⁵ L. Fu, C. L. Kane, and E. J. Mele, Phys. Rev. Lett. 98, 106803 (2007).

⁶ L. Fu and C. L. Kane, Phys. Rev. B **76**, 045302 (2007).

⁷ R. Roy, Phys. Rev. B **79**, 195322 (2009).

⁸ J. E. Moore and L. Balents, Phys. Rev. B **75**, 121306 (2007).

⁹ D. Hsieh, D. Qian, L. Wray, Y. Xia, Y. Hor, R. Cava, and M. Hasan, Nature **452**, 970 (2008).

¹⁰ M. Sato, Phys. Rev. B **73**, 214502 (2006).

- A. P. Schnyder, S. Ryu, A. Furusaki, and A. W. W. Ludwig, Phys. Rev. B 78 195125 (2008).
- ¹² R. Roy, arXiv:0803.2868 (unpublished).
- ¹³ X.-L. Qi, T. L. Hughes, and S.-C. Zhang, Phys. Rev. B **78**, 195424 (2008).
- ¹⁴ A. P. Schnyder, S. Ryu, and A. W. W. Ludwig, Phys. Rev. Lett. 102, 196804 (2009).
- ¹⁵ A. P. Schnyder, S. Ryu, A. Furusaki, and A. W. W. Ludwig, AIP Conf. Proc. **1134**, 10 (2009).
- ¹⁶ A. Y. Kitaev, AIP Conf. Proc. **1134**, 22 (2009).
- ¹⁷ X.-L. Qi, T. L. Hughes, S. Raghu, and S.-C. Zhang, Phys. Rev. Lett. **102**, 187001 (2009).
- ¹⁸ M. Sato, Phys. Rev. B **79**, 214526 (2009).
- ¹⁹ M. Sato and S. Fujimoto, Phys. Rev. B **79**, 094504 (2009).
- ²⁰ P. Hosur, S. Ryu, and A. Vishwanath, Phys. Rev. B 81, 045120 (2010).
- ²¹ X.L. Qi, T. L. Hughes, and S.-C. Zhang, Phys. Rev. B 81, 134508 (2010).
- S. Ryu, A. P. Schnyder, A. Furusaki, and A. W. W. Ludwig, New Journal of Physics 12 065010 (2010).
- ²³ N. Read and D. Green, Phys. Rev. B **61** 10267 (2000).
- ²⁴ M. R. Zirnbauer, J. Math. Phys. **37**, 4986 (1996).

- ²⁵ A. Altland and M. R. Zirnbauer, Phys. Rev. B **55**, 1142 (1997).
- ²⁶ C. Bruder, Phys. Rev. B **41**, 4017 (1990).
- ²⁷ C. R. Hu, Phys. Rev. Lett. **72**, 1526 (1994).
- ²⁸ Y. Tanaka and S. Kashiwaya, Phys. Rev. Lett. **74**, 3451 (1995).
- ²⁹ S. Kashiwaya, Y. Tanaka, M. Koyanagi, and K. Kajimura, Phys. Rev. B **53**, 2667 (1996).
- ³⁰ S. Kashiwaya and Y. Tanaka, Rep. Prog. Phys. **63**, 1641 (2000).
- M. Eschrig, C. Iniotakis, and Y. Tanaka, arXiv:1001.2486v1 (unpublished).
- We note that the gap functions (1d) and (1e) break the cubic symmetry of the normal state Hamiltonian h(k). A small symmetry-breaking term can be included in h(k), however, without changing the topological properties of the system, and so we have neglected this in our analysis in the interests of simplicity.
- It is important not to confuse the particle-hole symmetry of the Bogoliubov-de Gennes Hamiltonian, Eq. (1), with the electron-hole symmetry of the normal state band structure, Eq. (1c), at half filling (i.e., $\mu_j = 0$). The latter symmetry is irrelevant for the topological properties and does not play any role in our analysis.
- ³⁴ B. Beri, Phys. Rev. B **81**, 134515 (2010).
- ³⁵ S. Murakami and S. I. Kuga, Phys. Rev. B **78**, 165313 (2008).